Material Selection and Structural Analysis of an Undergraduate-Designed Unpowered Hypersonic Glide Vehicle

Grace Craft*, Alexander Berthelot†, and Aaron Matheny‡
University of Tennessee, Knoxville, Tennessee, 37996

This paper covers the material selection and structural design of Tachyon, a hypersonic vehicle designed by the Student Space Technology Association (SSTA) at the University of Tennessee Knoxville. The requirements for the design process were defined by the University Consortium of Applied Hypersonics (UCAH) for the 2025 Undergraduate Hypersonic Flight Design Competition. Tachyon is a high-lift-to-drag, unpowered hypersonic glide vehicle designed to be launched at Mach 8 and operate below an altitude ceiling of 9 km. The material selection process for this project was driven by research of historical hypersonic flights. In order to prioritize affordable manufacturing, accessible materials and design concepts were pursued. As part of the design process, thermal and structural analyzes were performed to validate that the mission requirements were met. Aerodynamic loads from a 23.5G maneuver were obtained from a Computational Fluid Dynamics (CFD) analysis using NASA's Fully UNstructured 3D (FUN3D) solver. Structural Finite Element Analysis (FEA) was performed using ANSYS Mechanical to validate the resulting fin loading from the 23.5G maneuver. Thermal FEA was performed using SolidWorks Simulation to evaluate the effectiveness of the integrated thermal protection system (TPS) on mitigating heat transfer to the payload and avionics bay.

I. Introduction

Hypersonic flight has been a major focus of research in the United States since NACA successfully launched the X-15 program in 1954 [1]. The X-15 was the first vehicle to explore the hypersonic flight regime in steady level flight, which lies beyond Mach 5 [2]. Further ambition led to the development of air-breathing engines, such as ramjets and scramjets, that allow sustained hypersonic flight. The development of hypersonic systems is becoming increasingly relevant in the scope of national defense. In response to the increasing demand for new hypersonic technology, the Department of Defense (DoD) created the Joint Hypersonic Transition Office (JHTO) with the intention of bolstering hypersonic Research and Development (R&D) and growing the workforce [3]. Additionally, JHTO created the University Consortium for Applied Hypersonics (UCAH) as a means of expanding hypersonic research within the sphere of academia [3]. In March 2025, UCAH announced their first undergraduate hypersonic design competition. The objective of the competition was to design an unpowered, high lift-to-drag (L/D), hypersonic projectile that operates at low altitudes [4].

Based at the University of Tennessee, Knoxville, the Student Space Technology Association (SSTA) is a student organization that specializes in rocketry and various technologies in the field of aerospace. Without any prior experience designing hypersonic systems, a group of 10 undergraduate students from the SSTA entered the competition alongside teams from over 30 universities. Over the course of four months, the team designed Tachyon, an unpowered hypersonic glide vehicle. As a result of the team's unyielding rigor in a

*Undergraduate Student, University of Tennessee Knoxville, AIAA Student Member 1869586
†Undergraduate Student, University of Tennessee Knoxville, AIAA Student Member 1605464
‡Undergraduate Student, University of Tennessee Knoxville, AIAA Student Member 1810514

complex, multidisciplinary field of study, Tachyon was selected as one of four winning design concepts in the conclusion of this national competition.

In response to the mission requirements defined by UCAH, the SSTA's hypersonic team took initial inspiration from previously successful hypersonic programs such as NASA's X-43 air-breathing Hyper-X plane and the Boeing X-51A Waverider. The final sizing of Tachyon's geometry was the result of an iterative design process using aero-thermal analysis tools. A meticulous material selection and structural design process was also required to ensure thermal survivability and structural integrity while prioritizing affordability through modern fabrication techniques, such as additive manufacturing. This paper will detail the material selection process and structural design portion of this project, as well as the thermal and structural analysis performed through Finite Element Analysis (FEA).

II. Concept of Operation

A. Mission Requirements

The Request for Proposal from UCAH is provided in Ref. [4] and called for an unpowered, high L/D, hypersonic projectile that operates between Mach 5-8 and below an altitude ceiling of 9 km. The vehicle is to be launched at Mach 8 from a system of the team's choosing, as the design requirements prioritize dynamic flight. Each component of the vehicle must exhibit thermal survivability throughout the entire flight, with a minimum impact velocity of Mach 2. The vehicle must also be thermally protected so that the internal temperature does not exceed 347 K. To demonstrate structural integrity, the vehicle must be able to withstand a maneuver at the altitude ceiling with a minimum load factor of 15G. Following these constraints, the vehicle should be designed to maximize range, affordability, and manufacturing feasibility.

B. Vehicle Geometry Overview

The dimensions of the final selected geometry of Tachyon are shown in Fig. 1. It is a wedge-derived lifting body with a six fin arrangement and a tapered tail. The orientation at zero angle of attack is defined as the point where the flat top is parallel with the freestream. The selected fin design was shaped to have extreme sweep angles and a 0.50 mm fillet on the Leading Edge (LE), dramatically improving thermal survivability while minimally increasing drag.

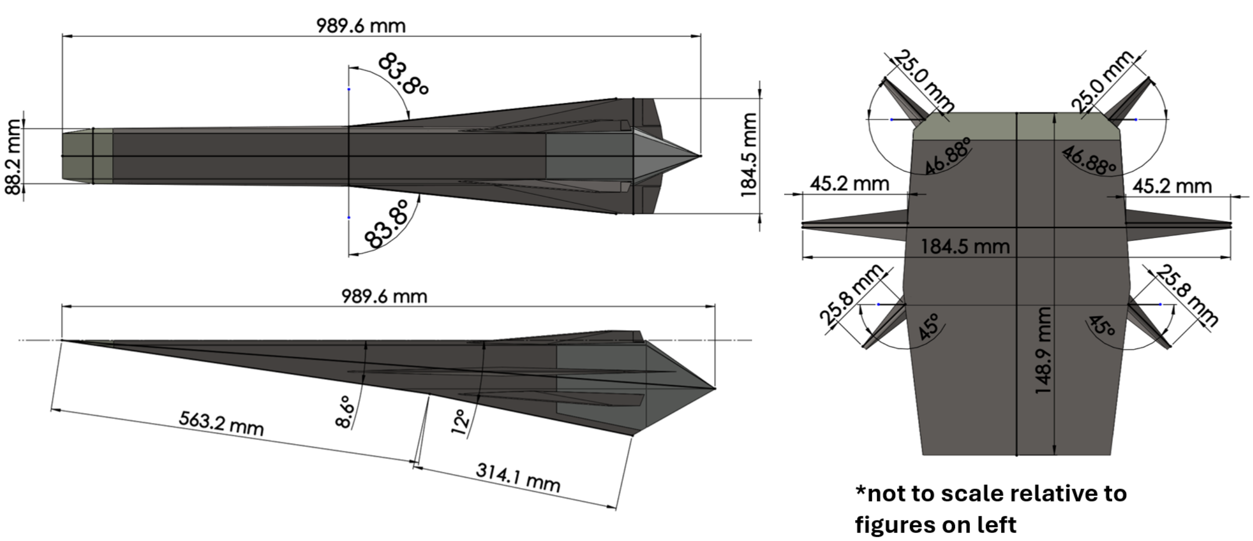

Fig. 1   External Geometry Dimensions

III. Design Process

A. Material Selection

The material selection process for Tachyon was inspired by the methods described by Bhat [5]. During the iterative design process of Tachyon's geometry, each section of the vehicle was examined, and general constraints were established based on prospective thermal and structural loading. The initial inspirations for materials to comprise Tachyon's LEs, primary structure, and Thermal Protection System (TPS) were found in the reports detailing historical flight technologies such as the X-15, X-51A, and X-43 [6]. The properties and applications of all material candidates were documented in a spreadsheet to streamline the selection process. Tachyon's flight parameters vary significantly from those of the historical vehicles studied, as it is a single-use craft that must not degrade while flying at high Mach numbers and low altitudes. A single, short flight mitigates the risk of structural failure due to creep and fatigue, so the design of a robust TPS that resists oxidation was prioritized [5].

Most materials utilized in the airframes of hypersonic technologies can be generalized into the primary categories of refractory metals, ceramics, or composites [7]. A large portion of Tachyon's material selection process was determining appropriate materials for its various LEs. As seen in historical technologies, advanced carbon-carbon (C/C) composites have been preferred to refractory metals due to their lower densities and higher service temperature ceiling [6]. The caveat to these advanced composites is the complex nature of manufacturing them. C/C technology is still under heavy development, with modern parts requiring the repetition of long procedures in order to achieve material properties capable of withstanding hypersonic environments [8]. Additionally, the performance of composite materials varies significantly depending on factors such as fiber orientation, matrix infusion methods, and post processing procedures [8]. For the purpose of producing an affordable design and simplifying analysis, composite materials were not chosen for this project.

The uses of Ultra-High Temperature Ceramics (UHTCs) were explored for potential applications to the TPS, as their resistance to oxidation is much higher than those of C/C and refractory metals [9]. As with C/C, the fabrication procedure is integral to maintaining properties that are appropriate for use in a LE [10]. Monolithic UHTC structures are considered to be brittle in nature, which discourages their use as primary load-bearing structures [9]. In terms of material cost, UHTCs are known to be expensive relative to the larger collective of materials considered for this project [9]. To optimize the cost and effectiveness of Tachyon's TPS, the use of UHTCs were only considered for protective coatings on parts of the vehicle that experience the highest risk of ablative oxidation.

Refractory metals and high-temperature alloys were selected to comprise the airframe since their material properties are predictable across varying fabrication techniques [11–13]. These materials are commonly used in additive manufacturing, which can produce complex geometries without sacrificing the integrity of the microstructure [13].

B. Structures

The mission requirement concerning structural integrity mandates the ability to withstand an aerial maneuver with a load factor of at least 15G. An internal truss-like structure was implemented to support the high magnitudes of stress placed on the vehicle. The airframe is segmented into sections that include trusses as part of their geometry. The majority of the airframe is composed of Inconel 718, a nickel-based super-alloy that maintains high strength and natural oxidation resistance at high temperatures [6, 14]. As for the tail and rear portion of the internal structure, a gamma-Titanium Aluminide (γ-TiAl) was selected for its lower density and comparable service temperature to Inconel [15]. Implementing a low density material in the rear of the vehicle aids longitudinal stability by shifting the Center of Gravity (CG) forward. Preliminary heating analysis was used to determine areas where γ-TiAl can be used without exceeding its service temperature.

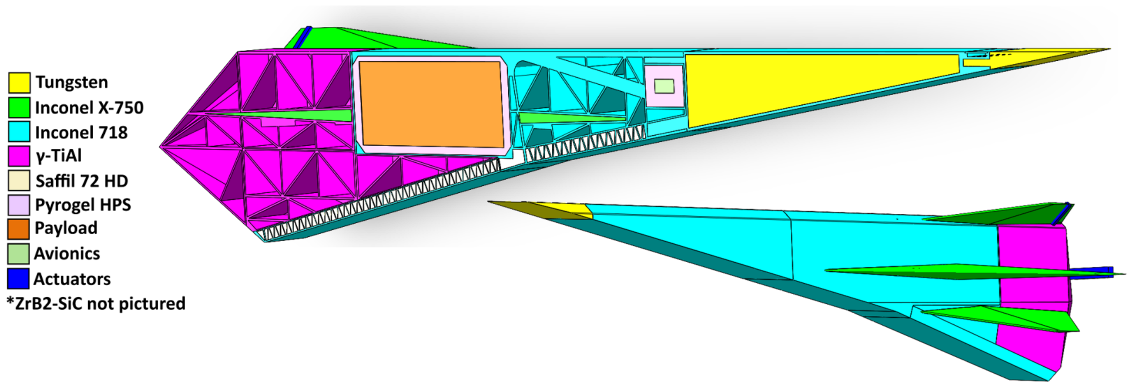

Fig. 2   Internal and External Structure Material Placement

Early iterations of Tachyon used tungsten LEs on the fins, but this was undesirable due to the difficulty of machining tungsten with such precision. As such, the fins were given large sweep angles and fillet radii to reduce heating on the structure. Since the LEs of the fins would still experience temperatures that fall into the melting range of Inconel 718, an alternative material is required to ensure thermal survivability. Inconel X-750 was selected as the material for all fins, since it exhibits a higher service temperature than Inconel 718 at the cost of a slight reduction of specific strength. [16][14]. Each fin contains a spar structure that is embedded into the airframe. The upper and lower fins have spars that span their root Chords (C_r), while the middle fins have a gap in the middle of their spars where the payload is located, as seen in Fig. 3. To add further mechanical support, the exterior of the payload chamber includes pegs that fit into the interior of the fin.

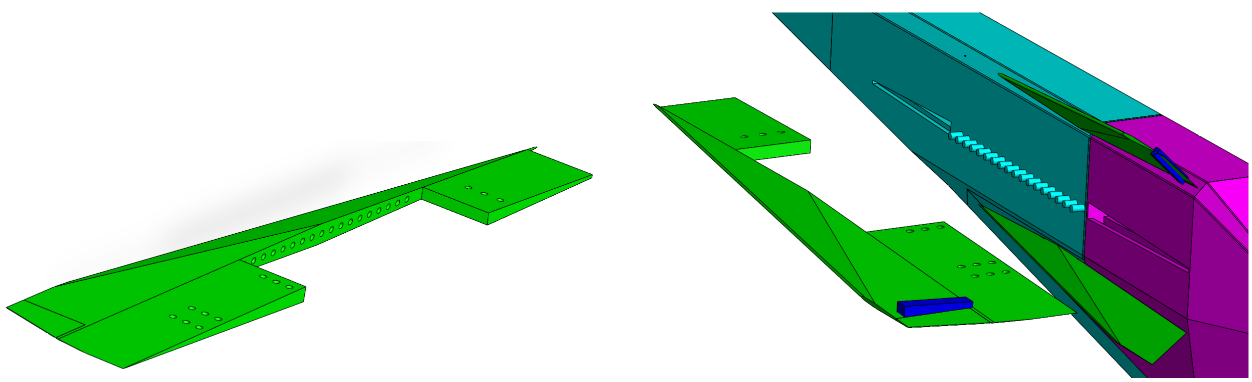

(a) Isolated View of Middle Fin Spar   **(b) Middle Fin Support on External Airframe**

Fig. 3   Middle Fin Spar Integration

Tungsten was selected to be the LE material on Tachyon's nose, since its maximum service temperature is high enough to withstand the extreme temperatures experienced at that point [6]. However, tungsten begins rapid oxidation at temperatures lower than those it would experience at the LE, and precision machining fillets is expensive with that material [6, 17]. For the simplification of manufacturing, the surface area of tungsten exposed to the flow environment is minimized. A thin coating made of Zirconium-Diboride and Silicon-Carbide (ZrB_2-SiC) was selected to protect the exposed tungsten from material degradation[6, 18, 19]. The tungsten nose tip is fastened to the Inconel portion of the nose with bolts as seen in Fig. 4. A larger piece of tungsten is secured within the nose frame in order to act as a counterweight to aid stability. Tungsten is also highly conductive which allows it to act as a heat sink to reduce heat transfer to the internal components [17].

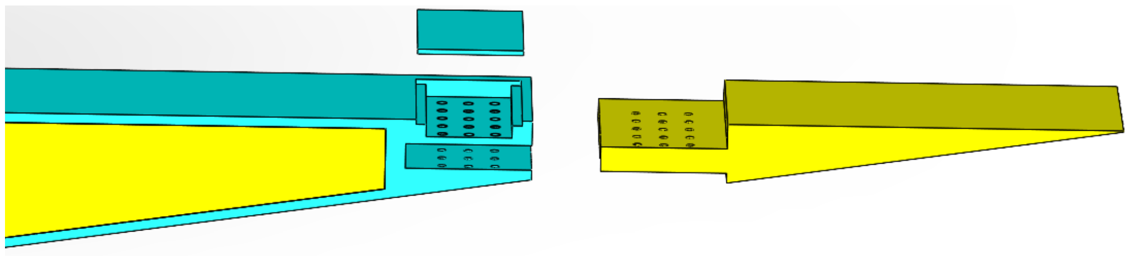

Fig. 4 Interior Nose Structure

C. Thermal Protection System

As the payload was shifted toward the hot underside of the wedge due to aerodynamic stability and geometric concerns, special consideration was placed on designing a TPS to prevent the maximum interior temperature from exceeding 347 K. Several approaches for a TPS were considered, including passive, semi-passive, and active designs [20]. Active and semi-passive TPS were not selected due to complexities arising in the design, manufacturing, and analysis of such structures, as the aerodynamic heating encountered by Tachyon in a single-use application was not enough to justify the design and fabrication of such a structure[21][22]. Ultimately, a passive hot structure approach was chosen, with the payload protected with fibrous insulation. A corrugated-core sandwich structure was added to the underside of the fuselage to more efficiently insulate the payload within the given space [23]. This approach is the least complex and most economical to manufacture, while also satisfying the design requirements. Saffil 72HD and Pyrogel HPS were chosen for the insulative TPS material for their low conductivities and high service temperatures. Saffil is commonly used in aerospace applications as a material for heat shields [24]. Pyrogel HPS is a silica-based aerogel insulation used in high temperature industrial applications to insulate pipes [25]. Although aerogel insulation is not widely used in the aerospace industry, Pyrogel HPS is proven as an industrial-grade insulator, and was thus deemed suitable to include in the TPS design. Since the tungsten portion of the nose will be vulnerable to rapid oxidation, a protective coating is required to counteract the effect. A ZrB_2-SiC UHTC coating was selected to serve this purpose [6, 18, 19]. The reinforcement and protection of components essential to the passive nature of the TPS ensures a thermally survivable design.

D. Cost and Manufacturing

The entire structure can be fabricated using modern additive manufacturing techniques. The selected materials are able to be printed into uniform sections of the airframe using Laser Powder Bed Fusion (L-PBF) technology [13]. Printing entire sections of the structure will significantly reduce lead times, labor costs, and the overall cost of manufacturing compared to traditional machining [13]. The mass of each material used and the corresponding costs can be found in Table 1. The two tungsten components are to be printed in their entirety, while the rest of the structure would be printed to form individual halves of the fuselage, divided by the centerline. This configuration ensures access to all parts of the internal structure so that the payload, avionics, and insulation components can be easily installed. The individual sections of the airframe can be secured together with bolts on the interior and sealed with high quality Electron-Beam Welding (EBW) [26]. The UHTC coating is fabricated via the Vacuum Plasma Spray (VPS) method. By weight, the coating consists of 75% ZrB_2 and 25% SiC [27]. The ZrB_2 and SiC start as powders that are pretreated through a ball milling and spray drying method to ensure consistent spherical particles [27][28]. The ZrB_2-SiC is then applied directly to the tungsten nose tip using the VPS method to form a thin, 200 μm, coating [29].

Table 1 Bill of Materials

Material	Location	Total Mass (kg)	Cost ($/kg)	Cost ($)	Manufacturing
Tungsten [30]	Nose, Leading Edge	15.278	157.00	2398.64	L-PBF
Inconel X-750 [31]	Wings	2.880	130.00	374.40	L-PBF
Inconel 718 [32]	External Surface	7.572	120.00	908.64	L-PBF
γ-TiAl [33]	Internal Structure and Rear Surface	2.014	150.00	302.10	L-PBF
Saffil 72 HD [34]	Insulation, Sandwich Structure	<0.01	53.98	<0.54	Commercial
Pyrogel HPS [35]	Payload Insulation	<0.1	61.00	<6.10	Commercial
ZrB_2 [36]	UHTC Coating	<0.02	556.67	<11.13	VPS
SiC [37]	UHTC Coating	<0.001	61.20	<61.00	VPS
Total Cost ($)				**4062.55**	

IV. Methodology

FEA was employed to fully characterize the thermal protection and survivability of the design. Boundary Conditions (BCs) for convective heat transfer were derived based on an aerodynamic database containing surface heating data collected from Reynolds-Averaged Navier-Stokes (RANS) Computational Fluid Dynamics (CFD) and wind tunnel testing in the University of Tennessee Space Institute's (UTSI's) Mach 7 Ludwieg Tube [38]. From these sources, heating data at flight conditions of interest detailed by table 3 were compiled and BC's were derived for transient thermal analysis.

Table 2 Case matrix for CFD aerodynamic database

M_∞	α	β
2.0, 4.0, 6.0	-5.0, 0.0, 2.5,	0.0, 5.0
7.0, 8.0	5.0, 10.0	

Table 3 Flow conditions for heating analysis

M_∞	Altitude (km)	Duration (s)
8.0	0.0	10.0
7.0	9.0	40.0
4.0	0.0	20.0

CFD analysis was performed with NASA's Fully UNstructured 3D (FUN3D) solver with flight conditions defined by table 2. Cases above Mach 4 were run with a one-temperature, five-species air, finite-rate reacting gas model. Cases below Mach 4 were run with a calorically perfect gas model. The one-temperature cases were run with Wilcox's $k-\omega$ turbulence model [39] and calorically perfect cases were run with Menter's baseline two-equation model [40]. A y^+ value of 0.10 was desired to sufficiently resolve heating. An average y^+ of 0.005 was calculated with a maximum of 0.31. To obtain specified convection BCs for transient FEA, both isothermal and adiabatic cases were run with the aerothermodynamic flight conditions specified in table 3 to derive the mean convection coefficient $\bar{h}$ and freestream temperature T_∞. A heat flux q_w'' was obtained from an isothermal case with specified wall temperature T_w, and the recovery temperature T_r was obtained from an adiabatic case. Convection coefficient was found as shown in equation (1).

$$\bar{h} = \frac{q_w''}{T_r - T_w} \quad \text{(Source: [41])} \tag{1}$$

BCs for FEA heat transfer in SolidWorks Simulation are derived from heating trends normalized to wind tunnel heating results. The full FEA case setup has 27 convection BCs with the most significant values shown in figures 5 and 6. Based on the trajectory estimates, the vehicle will decelerate below Mach 5 within 30 seconds. As a conservative approach to modeling the heat transfer, BCs from Mach 7 altitude 9 km are applied and run with a time-accurate scheme for 40 seconds with an initial temperature of 288 K.

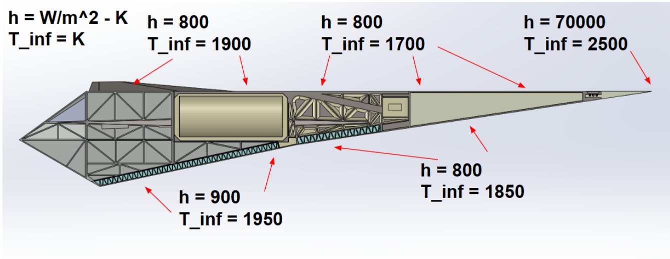

Fig. 5 Boundary conditions for payload and avionics bay insulation at Mach 7, altitude 9 km

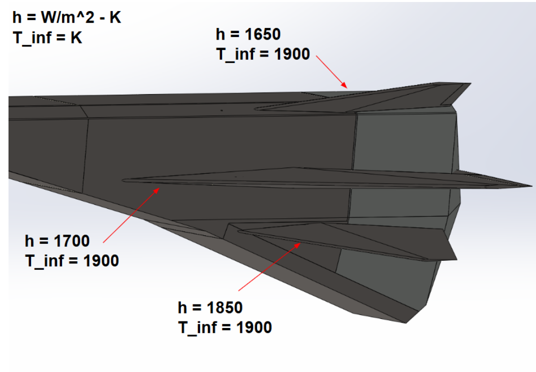

Fig. 6 Boundary conditions for fin leading edges at Mach 7, altitude 9 km

Fin loading conditions of the mid-flight pitch maneuver were obtained from FUN3D. A simulated maneuver with a 10 degree angle of attack (AOA) at Mach 7 at 9 km generated a load factor of 23.5 g. The CFD analysis provided aerodynamic pressure loads for each fin, given in Table 4. FEA for the structural analysis is carried out using ANSYS Mechanical. In the finite element model, only the middle fin was taken into account. The middle fin has the largest planform area (S) and largest pressure load of all the fins, so survival of the middle fin would indicate the survival of the rest of the fins. So, it was determined safe to omit the rest of the fins from the analysis. Actuators were also omitted from the analysis. Around 235000 nodes and 150000 elements were used for the model of the middle fin. A static structural analysis was performed to model the aerodynamic loading during the sustained 23.5G maneuver. The analysis is considered conservative, as the aerodynamic pressure loads are independent of time.

Location	Lift Force (N)	Pressure Load (kPa)
Top Fin	27.2	7.5
Middle Fin	266.0	21.6
Bottom Fin	35.4	10.0

Table 4 Aerodynamic BCs during 23.5 g maneuver with 10 degree AOA, at Mach 7 at 9km

Uniform pressure was applied to the underside of the middle fin, along with standard Earth gravity. The joints are assumed to be perfectly bonded, and topology is shared throughout the finite element model. Displacement of the fin spar is constrained in 6 Degrees of Freedom (DoF). To evaluate control surface deflection caused solely by the aerodynamic pressure loads, one side of the control surface was left free to deflect, while the other side is perfectly bonded to the rest of the fin. An environmental temperature of 1000 K is applied to reflect the elevated temperatures of the fin during flight, while eliminating the extraneous stresses due to thermal expansion at the interface of the fixed wing spar and the fin. Corresponding material properties for Inconel X-750 were added to reflect the weakened material properties during flight. Deformations and equivalent von Mises stresses were assessed to determine the structural survivability. The maximum stress on the middle fin is divided by the yield stress of Inconel X-750 at 1000 K to determine the factor of safety, and a factor of safety of 1.5 is required to fulfill the mission requirements [4].

Table 5 Material Properties [12, 17, 18, 24, 25, 32, 42, 43]

	Tungsten	Inconel X-750	Inconel 718	γ-TiAl	ZrB_2-SiC	Saffil 72 HD	Pyrogel HPS
Temperature Range (K)	300 - 2500	300 - 1145	294 - 1089	293 - 811	298 - 2273	873 - 1473	273 - 923
Density (kg/m ^{3})	19.3	8.26	8.22	4.41	5.33	0.145	0.20
Yield Strength (MPa)	2200	975 - 295	648 - 338	1098 - 527	217	-	-
Young's Modulus (GPa)	410	214 - 152	165 - 110	107 - 62	446 - 1.63	-	-
Specific Heat (J/kg-K)	129	431	421 - 652	582 - 730	407 - 765	1000	850
Conductivity (W/m-K)	167 - 62	14.1 - 24	12 - 18	8 - 11	65 - 53	0.11 - 0.30	0.02 - 0.07
Melting Point (K)	3660	1663	1523	1878	2573	2143	923

V. Analysis

A. Thermal Analysis

Transient heating analysis was performed in SOLIDWORKS Simulation to assess the viability of the TPS design and fin material selection. Figure 7 shows the temperature of the payload and avionics bays after being subjected to a head load corresponding to 40 s of heating at Mach 7 at the altitude ceiling. Based on the final trajectory, Tachyon will decelerate below Mach 7 within 5 s, so a heat load that corresponds to Mach 7 applied for 40 s is considered conservative. The contour minimum in Fig. 7 is set to 347 K, which is the upper limit for the payload. Figure 8 shows the temperature of the fins under the same heating conditions. The contour maximum in Fig. 7 is set to 1500 K, which is the melting point of Inconel X-750. Because the temperature of the payload and avionics bays is below 347 K, the TPS is shown to effectively insulate the interior of the vehicle, and thus satisfies the given mission requirements. Similarly, as the temperature of the fins do not exceed 1500 K after conservative heat loading, Inconel X-750 is demonstrated to be a suitable material to comprise Tachyon's fins.

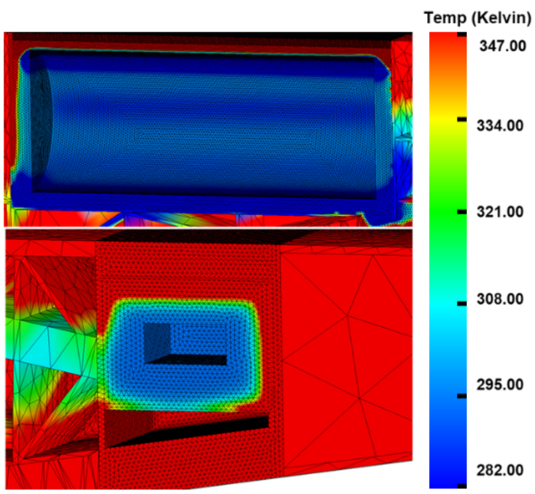

Fig. 7 Payload (top) and avionics (bottom) bays after 40 s of heating at Mach 7, altitude 9 km

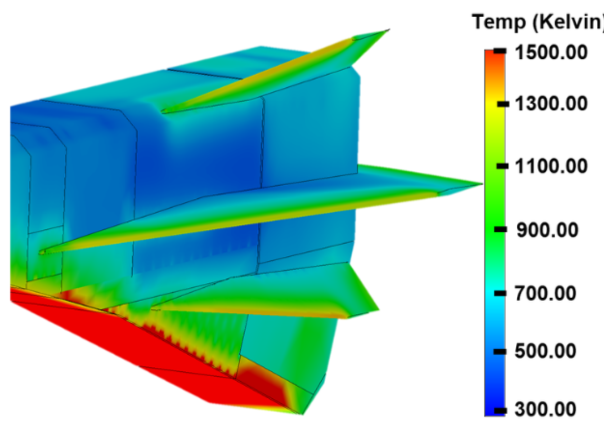

Fig. 8 Fins after 40 s of heating at Mach 7, altitude 9 km

B. Structural Analysis

Figure 9 shows the resulting stress and deformation experienced by the middle fin due to a uniform pressure load corresponding with the measured load factor. Structural FEA demonstrated that under this loading, the fins do not yield with a factor of safety of 3.5 relative to the yield stress of Inconel X-750 at 1000 K. The high factor of safety under the 23.5G load at the elevated temperature indicates Tachyon far exceeds the competition requirement of surviving a 15G load with a 1.5 factor of safety.

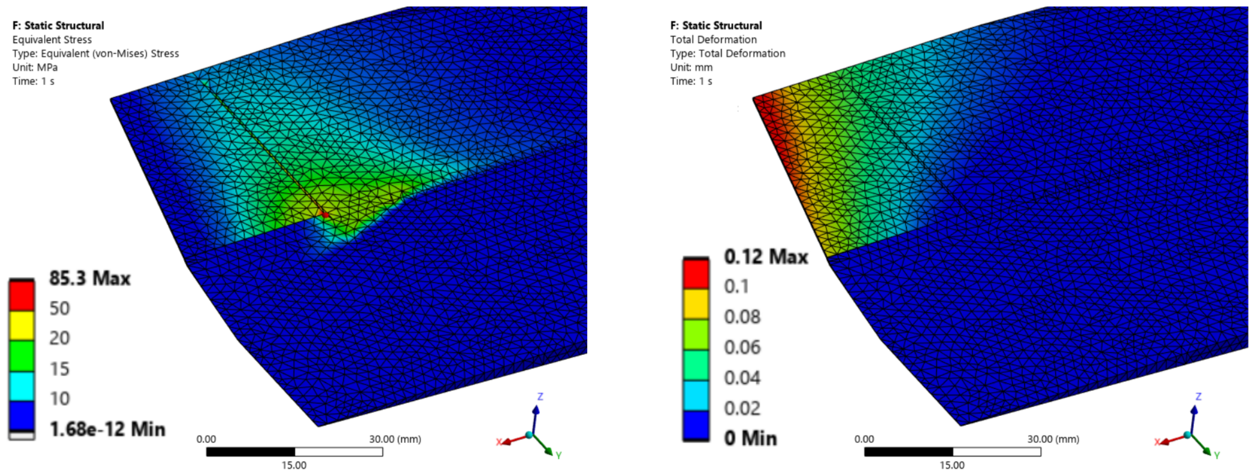

(a) Stress on middle fin under a 23.5G load **(b) Deformation of middle fin under 23.5G load**

Fig. 9 Middle Fin Loading Analysis

VI. Conclusion

In order to fulfill the project call to design an unpowered hypersonic flight vehicle, SSTA employed thorough research and analysis techniques to produce a structurally robust and thermally protected design. Material selection as a part of iterative design led to the conception of an airframe that consists solely of high temperature alloys and refractory metals that can be produced with additive manufacturing. Analyses were performed to validate the structural integrity of the vehicle and effectiveness of the TPS. The FEA performed on the primary lifting fin showed that the structure would not fail under the selected conditions with a factor of safety of 3.5. To accompany the resilient primary structure, the passive TPS protects the payload and avionics bay from extreme thermal loading, thereby satisfying the UCAH mission requirement. Conservative transient heating analysis, assuming Mach 7 conditions for 40 seconds, showed that the necessary internal components were kept below the desired temperature of 347 K. In the future, higher fidelity analysis can be utilized to influence design refinement.

Acknowledgments

This project would not have been possible without the support and technical guidance of Dr. Stefen Lindörfer. The Hypersonic Development Team at SSTA also thanks Dr. John Schmisseur, Dr. Cary Smith, and the entire faculty at the University of Tennessee Space Institute (UTSI) for their support of this project.

References

[1] NASA Langley Research Center, "Hypersonics – SACD VAB Projects," `https://sacd.larc.nasa.gov/vab/vab-projects/hypersonics/`, 2026. Accessed: 10-Feb-2026.

[2] NASA, "X-15: Hypersonic Research Program," `https://www.nasa.gov/reference/x-15/`, 2026. Accessed: 10-Feb-2026.
[3] U.S. Department of Defense, "DOD Establishes Joint Hypersonics Transition Office Systems Engineering Field Activity at NSWC Crane," `https://www.defense.gov/News/Releases/Release/Article/2382951/dod-establishes-joint-hypersonics-transition-office-systems-engineering-field-a/`, 2020. Accessed: 10-Feb-2026.
[4] Texas A&M University Hypersonics Laboratory, "2025 Undergraduate Hypersonic Flight Design Competition," `https://hypersonics.tamu.edu/2025-undergraduate-hypersonic-flight-design-competition/`, 2025. Accessed: 10-Feb-2026.
[5] Arnold, S. M., Cebon, D., and Ashby, M., "Materials Selection for Aerospace Systems," *Aerospace Materials and Applications*, edited by B. N. Bhat, American Institute of Aeronautics & Astronautics, 2018, Chap. 3.
[6] Peters, A. B., Zhang, D., Chen, S., et al., "Materials design for hypersonics," *Nature Communications*, Vol. 15, 2024, p. 3328. https://doi.org/10.1038/s41467-024-46753-3.
[7] Gilmer, D., "History of Hypersonic Materials," Presentation, University of Tennessee Knoxville, 2025.
[8] Muhammed, F., Lavaggi, T., Advani, S., Mirotznik, M., and Gillespie, J. W., "Influence of material and process parameters on microstructure evolution during the fabrication of carbon–carbon composites: a review," *Journal of Materials Science*, Vol. 56, No. 32, 2021, pp. 17877–17914. https://doi.org/10.1007/s10853-021-06401-3.
[9] Ni, D., Cheng, Y., Zhang, J., Liu, J.-X., Zou, J., Chen, B., Wu, H., Li, H., Dong, S., Han, J., Zhang, X., Fu, Q., and Zhang, G.-J., "Advances in Ultra-High Temperature Ceramics, Composites, and Coatings," *Journal of Advanced Ceramics*, Vol. 11, No. 1, 2022, pp. 1–56. https://doi.org/10.1007/s40145-021-0550-6.
[10] Johnson, S. M., "UHTC Research at NASA Ames," Presentation, Apr. 2011. Report Number: ARC-E-DAA-TN3427; Document ID: 20110014335; Public Use Permitted.
[11] Glass, D. E., Adams, J. W., and Fleet, M. A. V., "Materials Development for Hypersonic Flight Vehicles," *NASA Technical Report*, 2012. Focused summary of TPS, oxidation challenges, and structural design.
[12] Haynes International, "HAYNES® X-750 Alloy – Physical Properties Datasheet," Online, . URL https://haynesintl.com/en/alloys/alloy-portfolio/high-temperature-alloys/haynes-x-750/, accessed: 2025-12-09.
[13] Blakey-Milner, B., Gradl, P. R., Snedden, G., Brooks, M., Pitot, J., Lopez, E., Leary, M., Berto, F., and du Plessis, A., "Metal additive manufacturing in aerospace: A review," *Materials & Design*, Vol. 209, 2021, p. 110008. https://doi.org/10.1016/j.matdes.2021.110008.
[14] MatWeb, LLC, "Inconel 718 (UNS N07718) Nickel-Based Superalloy — Material Data Sheet," https://asm.matweb.com/search/specificmaterial.asp?bassnum=ninc34, 2025.
[15] Tenney, D. R., Lisagor, W. B., and Dixon, S. C., "Materials and Structures for Hypersonic Vehicles," Tech. Rep. ICIS-88-2.3.1, NASA Langley Research Center, Hampton, VA, 1988. Key review of structural materials and hot structure design for reusable hypersonic vehicles.
[16] *Inconel Alloy X-750: Properties, Composition, and High-Temperature Performance*, Special Metals Corporation, 2019. Material datasheet for Inconel X-750 used in high-temperature aerospace applications.
[17] NASA Ames Research Center, "Material Properties — Tungsten," https://tpsx.arc.nasa.gov/Material?id=62, 1995. Accessed: 2025-12-08.
[18] Purwar, A., and Basu, B., "Thermo-structural design of ZrB_2–SiC-based thermal protection system for hypersonic space vehicles," *Journal of the American Ceramic Society*, Vol. 100, No. 4, 2017, pp. 1618–1633. https://doi.org/10.1111/jace.14750.
[19] Gupta, K., Murtaza, Q., and Yuvraj, N., "Development of ZrB2–SiC Plasma-Sprayed Ceramic Coating for Thermo-chemical Protection in Hypersonic Vehicles," *Journal of Materials Engineering and Performance*, Vol. 33, No. 3, 2024, pp. 1401–1410. https://doi.org/10.1007/s11665-023-08043-9.
[20] Glass, D. E., "Thermal Protection Systems and Hot Structures for Hypersonic Vehicles," *Aerospace Materials and Applications*, edited by B. N. Bhat, American Institute of Aeronautics & Astronautics, 2018, Chap. 9. URL http://ebookcentral.proquest.com/lib/utk/detail.action?docID=29191765, accessed: 2025-12-08.
[21] Anthony, F. M., Dukes, W. H., and Helenbrook, R. G., "Internal Convective Cooling Systems for Hypersonic Aircraft," NASA Contractor Report NASA CR-2480, NASA Langley Research Center, Washington, D.C., Feb. 1975. Prepared by Textron Bell Aerospace Division, Buffalo, NY.
[22] Glass, D. E., "Heat-Pipe-Cooled Leading Edges for Hypersonic Vehicles," Presentation, Workshop on Materials and Structures for Hypersonic Flight, Jul. 2006. NASA Falcon Lead, NASA Langley Research Center.
[23] Wei, K., Wang, X., Yang, X., Qu, Z., Tao, Y., and Fang, D., "Heat transfer mechanism and characteristics of lightweight high temperature ceramic cellular sandwich," *Applied Thermal Engineering*, Vol. 154, 2019, pp.

562–572. https://doi.org/https://doi.org/10.1016/j.applthermaleng.2019.03.126, URL https://www.sciencedirect.com/science/article/pii/S1359431118369655.
[24] Saffil (Alkegen / Unifrax), "Saffil® Blankets – Product Information Sheet," Online PDF datasheet, . URL https://www.alkegen.com/wp-content/uploads/2025/09/Saffil-Blankets_A-5473_051425_GL.pdf, accessed 2025-12-09; Typical classification temperature 1600 °C, alumina-based polycrystalline wool blanket.
[25] Aspen Aerogels, Inc., "Pyrogel® HPS – Product Datasheet," Online PDF datasheeet, . URL https://www.aerogel.com/wp-content/uploads/2021/06/Pyrogel_HPS_Datasheet_English_v1.3.pdf, accessed: 2025-12-09.
[26] EB Industries, *Electron Beam Welding Inconel*, Farmingdale, NY, 2025. URL https://ebindustries.com/electron-beam-welding-inconel/.
[27] Xu, X., Pan, X., Niu, Y., Li, H., Ni, D., Huang, S., Zhong, X., Zheng, X., and Sun, J., "Difference evaluation on ablation behaviors of ZrC-based and ZrB_2-based UHTCs coatings," *Corrosion Science*, Vol. 180, 2021, p. 109181. https://doi.org/10.1016/j.corsci.2020.109181.
[28] Bartuli, C., Valente, T., and Tului, M., "Plasma spray deposition and high temperature characterization of ZrB_2–SiC protective coatings," *Surface and Coatings Technology*, Vol. 155, No. 2-3, 2002, pp. 160–168. https://doi.org/10.1016/S0257-8972(02)00037-9.
[29] Hu, C., Ge, X., Niu, Y., Li, H., Huang, L., Zheng, X., and Sun, J., "Influence of Oxidation Behavior of Feedstock on Microstructure and Ablation Resistance of Plasma-Sprayed Zirconium Carbide Coating," *Journal of Thermal Spray Technology*, Vol. 24, 2015, pp. 1302–1311. https://doi.org/10.1007/s11666-015-0307-2.
[30] Shanghai Metals Market, "Tungsten Powder Price, USD/kg," https://www.metal.com/Tungsten/201308090022, 2025. Accessed December 8, 2025.
[31] MET3DP, "Nickel Alloy X750 Powder — Product Data Sheet," https://met3dp.com/product/nickel-alloy-x750-powder-20240124/, 2025. Accessed December 8, 2025.
[32] MET3DP, "Inconel 718 Powder — Product Data / Price Sheet," https://met3dp.com/inconel-718-powder-price-20231026/, 2025. Accessed December 8, 2025.
[33] MET3DP, "Titanium Aluminide Powder — Product Data Sheet," https://met3dp.com/titanium-aluminide-powder-20231213/, 2025. Accessed December 8, 2025.
[34] Le, V. T., Ha, N. S., Goo, N. S., and Kim, J. Y., "Insulation System Using High-Temperature Fibrous Insulation Materials," *Heat Transfer Engineering*, Vol. 40, No. 17-18, 2019, pp. 1523–1538. https://doi.org/10.1080/01457632.2018.1474602.
[35] IC Market, "Aerogels — mata izolacyjna Porogel Plus Pyrogel HPS," https://icmarket.pl/aerogels-mata-izolacyjna-porogel-plus-pyrogel-hps-pl.html, . Accessed: 2025-12-07.
[36] Metals, M., "Zirconium Diboride Powder," https://micronmetals.com/product/zirconium-diboride-powder/, . Accessed: 2025-12-07.
[37] McMaster-Carr, "Silicon Carbide Powders — Ceramic 3," https://www.mcmaster.com/products/silicon-carbide-powders/ceramic-3~/, . Accessed: 2025-12-08.
[38] University of Tennessee Space Institute, "Mach 7 Ludwieg Tube," , 2026. Available at https://www.utsi.edu/horizon/facilities/mach-7-ludwieg-tube/, accessed Feb. 4, 2026.
[39] Wilcox, D. C., "Formulation of the k-ω Turbulence Model Revisited," *AIAA Journal*, Vol. 46, No. 11, 2008, pp. 2823–2838. https://doi.org/10.2514/1.36541.
[40] Menter, F. R., "Two-Equation Eddy-Viscosity Turbulence Models for Engineering Applications," *AIAA Journal*, Vol. 32, No. 8, 1994, pp. 1598–1605. https://doi.org/10.2514/3.12149.
[41] van Driest, E. R., "The Problem of Aerodynamic Heating," Los Angeles, California, 1956. Presented at the Aerodynamic Heating: Aerodynamic Aspects Session, National Summer Meeting, IAS, Los Angeles, June 18-21, 1956.
[42] ANSYS, Inc., "ANSYS Mechanical: Engineering Data Material Library," https://www.ansys.com, 2025. Release 2025 R1.
[43] Emiralioglu, A., and Ünal, R., "Additive manufacturing of gamma titanium aluminide alloys: a review," *Journal of Materials Science*, Vol. 57, No. 7, 2022, pp. 4441–4466. https://doi.org/10.1007/s10853-022-06896-4.